J Mater Sci (2018) 53:14964–14974

Biomaterials

Hollow ZnO from assembly of nanoparticles: photocatalytic and antibacterial activity

Zakiullah Zaidi[1], Kalpesh Vaghasiya[1], Aditi Vijay[1], Manu Sharma[1], Rahul Kumar Verma[1], and Sonalika Vaidya[1,*]

[1] *Institute of Nano Science and Technology, Habitat Centre, Phase-X, Mohali, Punjab 160062, India*

Received: 11 April 2018
Accepted: 17 July 2018
Published online: 24 July 2018

ABSTRACT

Hollow shells of ZnO were formed by the assembly of nanoparticles using PEG 400 wherein PEG-400 acted like both a solvent and a structure directing agent. The structure, morphology and optical properties were characterized by using PXRD, SEM, TEM and absorption studies. The hollow shells were found to possess high crystallinity with a surface area of 8 $m^2 g^{-1}$. The assembly was formed by nanoparticles ranging from 50 to 60 nm, whereas the size of the hollow shell ranged from 500 nm to 1 micron. Photocatalytic activity of these nanostructures was studied using Rhodamine B (RhB) and methyl orange (MO). Nearly 99% of the RhB dye was found to be degraded in 60 min while for MO, the degradation was 97% in 50 min. The pseudo-first-order rate constant was calculated as 0.072 min^{-1} for the degradation of RhB and 0.075 min^{-1} for the degradation of MO. The hollow shells were found to exhibit significant bacterial inhibiting efficacy at a low concentration of the particles. Comparative studies were carried out for photodegradation of Rhodamine B dye and antibacterial activity using spherical particles of ZnO and assembly of particles to form rods of ZnO. The results indicated that these hollow nanostructures could be used as a potential catalyst for the removal of dyes from water and as an antibacterial agent.

Introduction

ZnO is a wide bandgap II-VI semiconductor. ZnO has a large band gap due to which it finds application, especially in the field of the dye-sensitized solar cell, photocatalysis, etc. Morphology, apart from the size of the nanostructures, plays an important role on the properties of the material. Various kinds of morphology can arise as a result of self-assembly of small building blocks. The hierarchical structures that are formed from the self-assembly of micro- and nanostructured building blocks (nanoparticles, nanorods, nanoplates and nanoribbons) possess high surface area, porosity and open active sites making them very attractive for catalysis. The assembled nanostructures provide much more exposed surface

Address correspondence to E-mail: svaidya@inst.ac.in

https://doi.org/10.1007/s10853-018-2715-4

region, facilitating the adsorption and photoreaction of reactants.

Role of the morphology of the nanostructures on photocatalytic activity of ZnO toward organic dye degradation has been studied widely. For instance, Kim et al. [1] showed variation in photocatalytic activity toward degradation of Rhodamine 6G for ZnO with varied morphologies, viz. rod-, peanut-, dumbbell-, and notched spheres-like. They found that rod-like ZnO showed high photocatalytic activity. Gupta et al. [2] observed that nanoparticles of ZnO exhibited higher photocatalytic activity toward degradation of methylene blue when compared with other morphologies of ZnO, viz. nanoparticles, nanorods, porous nanoassembly, microrods and microdisks. In another study carried out by Hui et al. [3], sea urchin-shaped Fe-doped ZnO nanostructures were found to degrade an aqueous solution of Rhodamine B dye. The photodegradation was found to be maximum for 5% doping of Fe in ZnO. Similarly, there are numerous studies on the effect of morphology on photocatalytic activity using ZnO [4–9].

From last so many decades, antibiotics have been employed to treat the hospital- or community-acquired infections. Recent advancement in the field of nanobiotechnology, especially the fabrication of novel metal oxide nanostructures with desired size and shape, has shown more significant antibacterial properties. When the metal oxide is synthesized in the form of functional nanostructures or nanoparticles having its diameter $\geq$ 100 nm on one axis, unique biophysicochemical properties useful in various fields, particularly in bio-nanomedicine, are observed [10, 11]. Various metal oxides like zinc oxide (ZnO), magnesium oxide (MgO) and titanium dioxide (TiO_2) have been approved by US Food and Drug Administration (21CFR182.8991) (FDA, 2011) as safe to human beings. The antibacterial activity of metal oxides has been primarily studied against human pathogenic Gram-negative and Gram-positive bacteria such as *Escherichia coli (E. Coli), Salmonella enterica (S. Enterica)* and *Staphylococcus aureus (S. Aureus)*. The significant factors like size, stability and concentration of metal oxide nanostructures mainly influence the antibacterial activity [12, 13]. Due to their high surface area to volume ratio, metal oxide nanostructures tend to interact with a variety of biomolecules such as proteins, DNA, lipids. On interaction with the biomolecules, the oxides produce free metal ions or reactive oxygen species (ROS) which react with the lipids of the integral membrane. These species cause disruption of the bacterial cell membrane leading to leakage of cytoplasmic contents. Nevertheless, the exact mechanism(s) behind the antibacterial activity of metal oxide nanostructures remains unclear. We site here few reports on the antibacterial activity of ZnO. Azam et al. [12] demonstrated that ZnO has better antibacterial properties when compared to CuO and Fe_2O_3. Vidovic et al. [10] showed that ZnO nanoparticles have a toxicity effect on the growth of *S. Enterica*. Studies on the effect of ZnO-PVC films [13] with varied concentration were carried out on the growth of *E. Coli* and *S. Aureus*. Biocidal activity of ZnO was observed by Padmavathy et al. [14], wherein the authors found that the efficacy of ZnO nanoparticles increases with a decrease in particle size. Manna et al. [15] showed that the size of the oxide plays a significant role on the antibacterial activity of the oxide. Toxicity/antibacterial activity is also found to be dependent on the shape and size of the nanostructures. Talebian et al. [16] in their study, on the effect of morphology on an antibacterial activity, found that flower-like morphology of ZnO was more efficient as compared to other morphology that is hexagonal rod-like and spherical-like ZnO. Liu et al. [17] in their study showed that nanocomposites of ZnO and graphene quantum dots possess a higher activity as an antibacterial agent *(for E.Coli and S. Aureus)* under UV light when compared to ambient light.

Hollow nanostructures are attractive for catalytic activity because of their high surface area and excellent permeability for the reactants. Lu et al. [18] showed that magnetic hollow spheres of carbon can be used for the removal of chromium ions. Hollow spheres of ZnO and ZnO–CuO composite hollow spheres were shown to degrade methylene blue [19]. Spherical shells of ZnO were also used for the degradation of phenol in aqueous solutions [20]. It has been reported in the literature that by using hollow spheres of WO_3, RhB dye could be degraded faster than other morphologies [21]. Jiexiang Xia and group compared the photocatalytic efficiency of BiOI hollow microspheres and nanoplates [22]. They observed that 92% of MO could be degraded when hollow microspheres were used as a photocatalyst. The degradation was found to be only 21% within 180 min of irradiation with visible light for nanoplates. Liu et al. [23] showed that hollow nanostructures of ZnO decorated with Ag were more effective

for photodegradation of dyes. These nanostructures also showed antibacterial activity toward *E. Coli* and *S. Aureus* based on synergistic bactericidal effect between Ag nanoparticles and ZnO. Apart from the reports mentioned above, there have been many reports on the use of hollow nanostructures as photocatalysis [24–26].

In this paper, we have tried to synthesize hollow ZnO (formed by the assembly of ZnO particles) using PEG 400 as the structure directing agent and have carried out its photocatalytic activity and toxicity studies on *E.Coli* and *S. Enterica*. Here, we have demonstrated the efficacy of the assembly of ZnO nanoparticles to hollow shells for removing dye and as an antibacterial agent by carrying out comparative studies using two other different kinds of morphology/assembly, viz. spherical particles and assembly of particles to form rods of ZnO. Removal of dyes from water is essential as these synthetic organic components are a threat to the environment. The dyes are stable and are resistant to aerobic degradation. Semiconducting oxides as photocatalyst help in their photodegradation. We have shown that these hollow nanostructures of ZnO have a high potential to be used as both photocatalytic and antibacterial coating material for broad applications, especially in food packaging industries, water purification, etc.

Materials and methods

Synthetic methodology

The reaction procedure was followed as reported in the literature [27] with some modification. 10 mmol of zinc nitrate hexahydrate (Sigma-Aldrich) was dissolved in 100 mL of polyethylene glycol 400 (Merck, India). The solution was then heated to 160 °C for 6 h after which it was cooled to room temperature. The resultant precipitate was collected by centrifugation and washed firstly with water followed by acetone. The precipitate was heated at 500 °C for 4 h to obtain an assembly of nanoparticles to form hollow shells of ZnO. For convenience, this is referred to as ZNO1. For carrying out comparative studies, ZnO with two different morphologies/assemblies, viz. spherical-shaped particles (ZNO2) and particles assembled to form rods (ZNO3), was synthesized. ZNO2 was synthesized using the co-precipitation method. Briefly, 50 mL of 0.2 M aqueous solution of zinc nitrate hexahydrate was taken. To this, 50 mL of an equimolar aqueous solution of ammonia was added. The mixture was stirred for 2 h. The precursor was obtained by centrifugation and washed with acetone. The precursor was heated at 300 °C for 6 h to obtain spherical particles of ZnO. For the synthesis of ZNO3, zinc oxalate nanorods synthesized using the reverse micellar method [28] were heated at 850 °C for 12 h to obtain particles assembled to form rods.

Characterization

The crystallinity and the phase purity of ZnO were checked using Powder X-Ray Diffraction (PXRD) using Eco D8 Advance Bruker XRD with a Cu Kα radiation source (λ = 0.15406 nm) operated at 40 kV and 25 mA at a scanning step of 0.02 in the 2θ range 10–80 degree. The morphology of zinc oxide nanoparticles was checked on powder mounted on carbon tape coated with gold, using scanning electron microscope (SEM) JSM-1T300 and JEOL 7600F field emission scanning electron microscope (FESEM). TEM studies were carried out with JEOL, JEM-2100, electron microscope operating at an accelerating voltage of 200 kV. The sample was prepared by dispersing the powder in absolute ethanol and drop casting the dispersion on a carbon-coated copper grid. Infrared (IR) spectroscopy studies were carried out on Agilent CARY-660 Fourier transform infrared (FTIR) spectrometer. The data were recorded with a KBr disk in the range of 400–4000 cm^{-1}. Diffuse reflectance spectra of the solid samples were recorded on UV–visible spectrophotometer Shimadzu UV-2600, which was operated in solid-state mode in the wavelength range of 250–800 nm with barium sulfate as the reference. Nitrogen adsorption–desorption isotherms were recorded at liquid nitrogen temperature (77 K) with Quanta Chrome Model Q2 equipment, and the specific surface area was determined by the Brunauer–Emmett–Teller (BET) method.

Photocatalytic activity

For the photocatalytic degradation of Rhodamine B and methyl orange, 100 mg of the catalyst was dispersed in 100 mL of 9 μM (RhB) and 12 μM (MO) dye solution and the mixture was irradiated with UV light using a high-pressure Hg lamp (250 W). The photocatalytic reactor was equipped with a water

circulating jacket. The adsorption capacity of the material was checked by allowing the sample to equilibrate in the dye solution for 30 min under dark conditions. After 30 min of stirring in the dark, the light source was switched on. The photodegradation of Rhodamine B/MO dye in aqueous solution was monitored using the UV–visible spectroscopy.

For showcasing the effectiveness of hollow nature of assembly on the photocatalytic activity, photodegradation of Rhodamine B was carried out using ZNO2 and ZNO3.

Antibacterial activity

The in vitro antibacterial activity of ZnO nanostructures (ZNO1, ZNO2 and ZNO3) was evaluated against *Salmonella enterica* and *E.Coli* bacteria using colony-forming unit plating assay method. Few colonies of *S. Enterica* and *E.Coli* were stripped from the standard Luria–Bertani (LB) agar plate which was separately inoculated in sterile nutrient broth media. The bacterial suspension was kept overnight in a shaker incubator at 120 rpm with a maintained temperature of 35 ± 3 °C to achieve the desired bacterial growth. Different concentrations of ZnO nanostructure (1–15 mg mL^{-1}) were treated individually with *S. Enterica* (~ 2.8×10^6 CFU/mL) and *E.Coli* (~ 3.2×10^6 CFU/mL) for 6 h at 35 ± 3 °C with continuous agitation (250 rpm) in an incubator shaker and checked for the inhibition of bacterial growth after incubation with prepared nanostructures. Phosphate-buffered saline was used as a negative control while ampicillin (50 µg/mL) was used as a positive control. Serial dilutions of treated bacteria were done for each treatment group in a total volume of 1 mL of PBS (pH 7.4). 1 mL aliquot of *E. Coli* was spread over 3 M Petrifilm *E. Coli* count (EC) plates while 100 µL of *S. Enterica*-containing sample was inoculated on LB agar plates. The plates were incubated overnight at 35 ± 3 °C in the shaking incubator for 24 h. The inhibition of bacterial growth was evaluated by counting viable colonies (CFU/mL). All antimicrobial assays were performed in triplicate and were done at least two different times to ensure reproducibility.

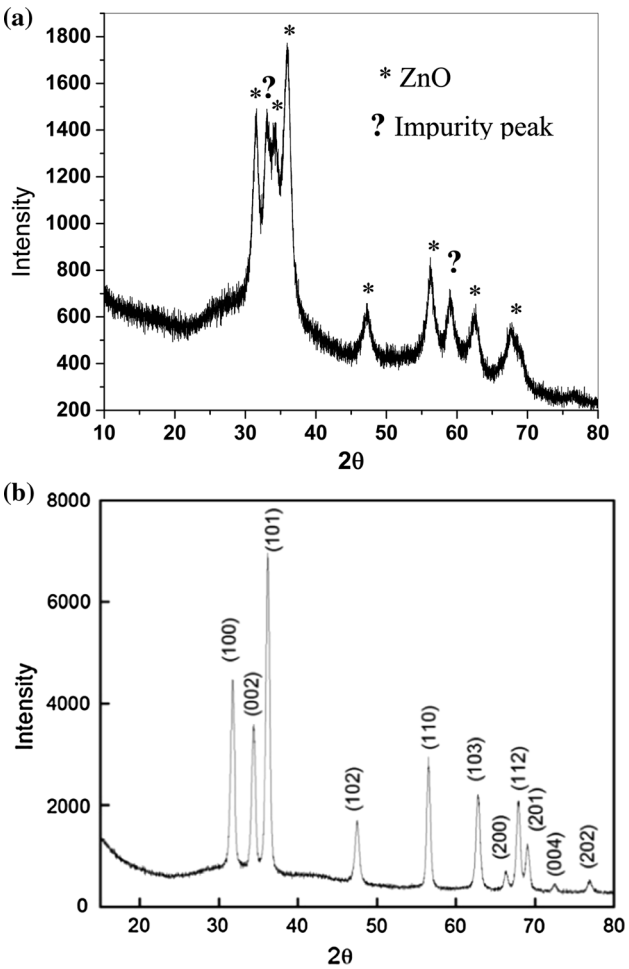

Figure 1 PXRD pattern of **a** precursor obtained by heating zinc ions in PEG 400 at 160 °C and **b** zinc oxide obtained after heating the precursor at 500 °C (ZNO1).

Result and discussions

The PXRD pattern of precursor obtained by heating zinc ions with PEG 400 at 160 °C is shown in Fig. 1a. ZnO with wurtzite structure along with few impurity peaks could be observed in the PXRD pattern. ZnO synthesized by heating the precursor at 500 °C (ZNO1) (Fig. 1b) shows the formation of the crystalline phase of ZnO with wurtzite structure. As observed from the intensity of the PXRD pattern, it can be perceived that the crystallinity of the hollow assemblies was found to increase when compared to that of the precursor. The PXRD pattern of ZnO obtained using co-precipitation method (ZNO2) (figure S1a) and by heating oxalate nanorods (ZNO3) (figure S1b) was found to crystallize in wurtzite structure and possessed high crystallinity.

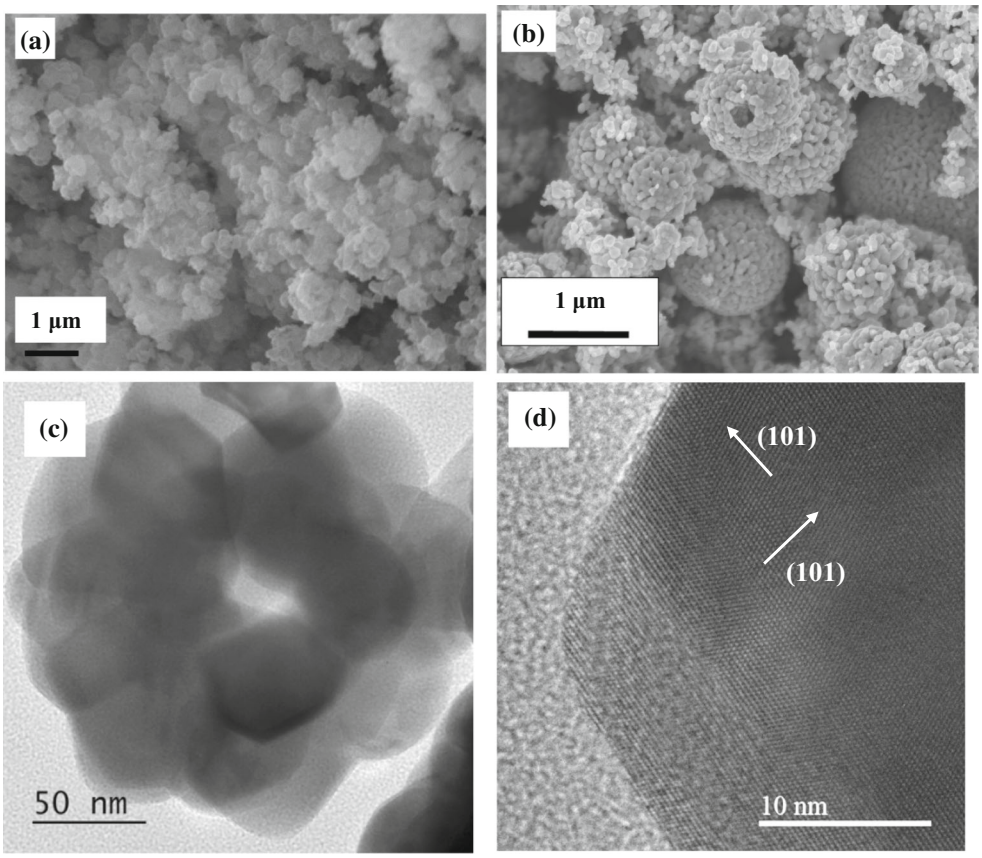

Figure 2 SEM image of **a** precursor obtained by heating zinc ions in PEG 400 at 160 °C and **b** ZnO hollow structures obtained after heating the precursor at 500 °C (ZNO1). **c** TEM image and **d** HRTEM image of ZnO hollow structures obtained after heating the precursor at 500 °C (ZNO1).

SEM image (Fig. 2a) of the precursor obtained by heating zinc ions and PEG 400 shows the formation of spherical particles. No assemblies were observed from the SEM image of the precursor. SEM image of ZNO1 shows particles assembled to form hollow shells (Fig. 2b). The size of the nanoparticles forming the assembly was 50–60 nm while the size of the hollow structures formed from the assembly was 500 nm–1 µm. Hollow nature of the assembly (ZNO1) is apparently visible from the cavity of the broken shell as observed in the SEM image (Fig. 2b).

TEM studies of ZNO1 (Fig. 2c) show that the particles of size 50 nm are assembled to form a cavity between the assemblies. This also suggests the formation of hollow shells formed from the assembly of the particle. Thus, the results corroborated with the SEM studies. HRTEM of ZNO1 shows (101) plane of ZnO (Fig. 2d). FTIR studies were carried out for both, the precursor obtained by heating zinc ions with PEG 400 at 160 °C (figure S2a) and zinc oxide after heating the precursor at 500 °C (ZNO1) (figure S2b). From figure S2a, bands corresponding to PEG 400 (ν_{O-H}: 3436 cm^{-1}, ν_{C-H} stretching: 2929 cm^{-1}, ν_{C-H} bending: 1598 cm^{-1}, ν_{O-H} bending: 1419 and 1319 cm^{-1}, ν_{C-O-C}: 1091 cm^{-1}) could be observed along with Zn–O vibrational frequency at 447 cm^{-1} suggesting that PEG 400 molecules are associated with the oxide. The bands corresponding to PEG 400 were not observed for ZNO1 (figure S2b), whereas a prominent band corresponding to ν_{Zn-O} was observed at 439 cm^{-1} indicating complete removal of the organic moiety in the heated sample. Thus, based on the above, the formation of the assembly can be explained on the basis of the structural directing influence of PEG 400. PEG-400 played a dual role during the synthesis. Firstly, it acted as a solvent wherein it is proposed that the Zn^{2+} ion in the solution formed a complex with PEG-400. PEG is known to form a complex with several lanthanides and transition metal cations and thus bears a good solvating property [29]. Secondly, it acted as a structure directing agent wherein, upon heating, the ions were hydrolyzed in the reaction

medium to form particles bound by PEG molecules. After annealing at 500 °C, all the PEG molecules were removed (as evident from the FTIR studies shown in figure S2b) resulting in the formation of hollow structures formed by the assembly of particles. The polymeric chain of PEG bears alternate hydrophilic and hydrophobic moiety which could have assisted in assembling of the particles. A schematic diagram showing the formation of the assembly of ZnO is shown in Fig. 3. Zhou et al. [27] carried out the synthesis of ZnO using PEG 200. We wish to highlight here that just changing the structure directing agent from PEG 200 to PEG 400 (i.e., changing the number of oxyethylene group) led to change in the nature of the hollow structure of the material. With PEG 200 [27], microspheres with rough and porous external surface were formed. In our study, the hollow structure was formed by the assembly of nanoparticles of ZnO. The change in the nature of hollow nanostructure could have arisen because of the increased number of oxyethylene groups in PEG 400. Also, it is a known fact that as the molecular weight of PEG increases, the steric effect of the polymer increases [29]. This increase in the steric effect of the polymer could have assisted in the formation of an assembly to form hollow nanostructure. Thus, the studies highlight that a simple change in the chain length of the polymer (keeping all other parameters constant that are involved in the synthesis) could lead to a significant change in the nature of assembly of the nanostructured material. The specific surface area of the assembled hollow nanostructures was found to be 8 m^2 g^{-1}. The band gap was found to be 3.20 eV for ZNO1, 3.19 eV for ZNO2 and 3.12 eV for ZNO3 which suggest that these assembled nanostructures will be photoactive in the UV region of the solar spectrum.

Photocatalytic activity

In order to check the photocatalytic degradation of the dye in the absence of a catalyst, the blank dye was irradiated with the light source. Absorption studies on blank dye were carried out at different time intervals for 1 h. It was observed that after 65 min of irradiation, only 19% of the dye (figure S3) degraded in the absence of catalyst, suggesting that the catalyst played a major role in photodegradation of the dye. Photocatalytic performance of ZnO nanostructures was demonstrated by using the degradation of Rhodamine B dye (RhB) and methyl orange (MO). A decrease in the peak intensity with time shows that the concentration of the dye decreased with time and the catalysts were photoactive. It was observed that nearly 99% of the RhB dye degraded in 60 min (Fig. 4a) when the hollow structure was used as a photocatalyst. For MO, the amount of dye that was photodegraded was 97% in 50 min (Fig. 4b). The photocatalytic degradation of the dye followed first-order kinetics with a rate constant calculated as 0.072 min^{-1} for RhB dye and 0.075 min^{-1} for MO (inset of Fig. 4a and 4b). In order to confirm the effectiveness of the hollow nature of the assembly as a photocatalyst, studies were carried out using ZNO2 and ZNO3 for photodegradation of Rhodamine B. It was observed that 94% of the dye could be degraded in 60 min with pseudo-first-order rate constant as 0.042 min^{-1} when ZNO2 (Fig. 5a) was used as photocatalyst. It is to be noted that the morphology of ZNO2 was spherical as evident from the SEM studies (figure S4a). TEM studies showed that the size of

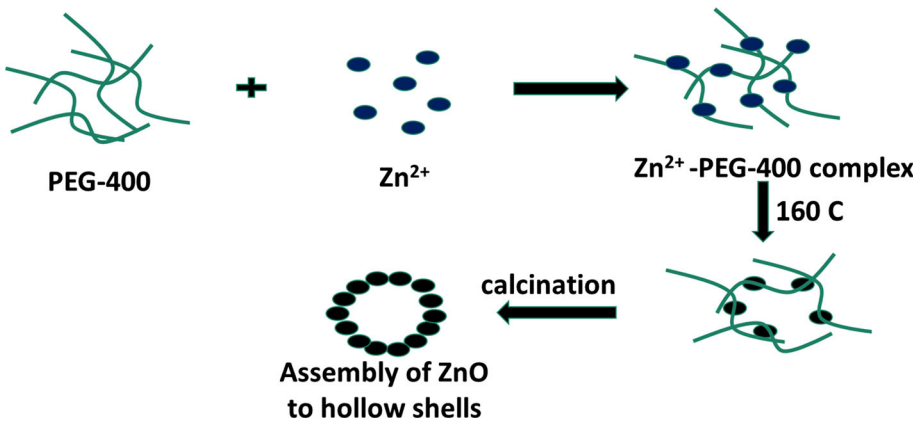

Figure 3 Schematic diagram showing the formation of ZnO hollow structure using PEG-400.

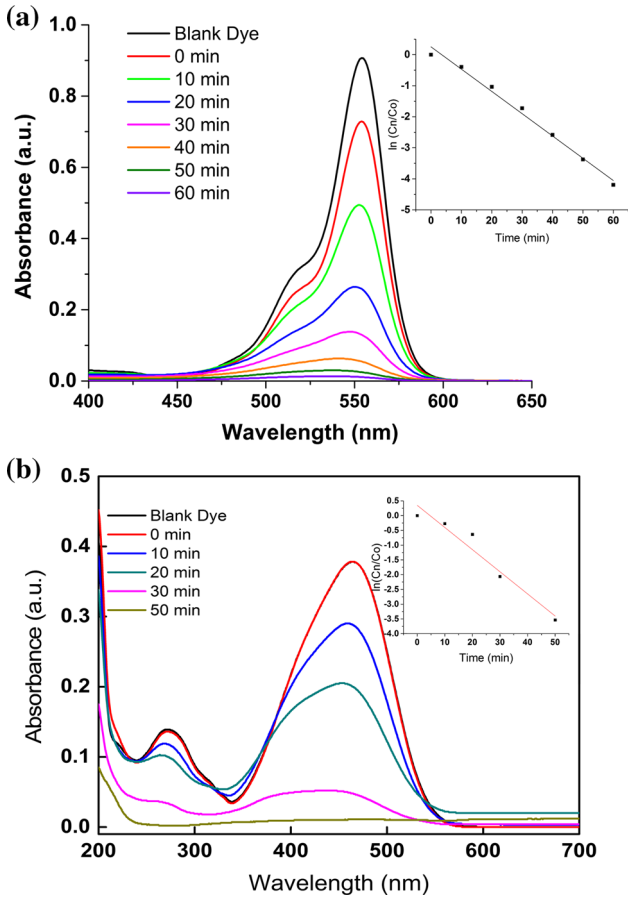

Figure 4 Photodegradation of **a** Rhodamine B and **b** methyl orange using an assembly of ZnO nanoparticles forming hollow structures (ZNO1). The inset shows the plot showing that the catalysis followed first-order kinetics.

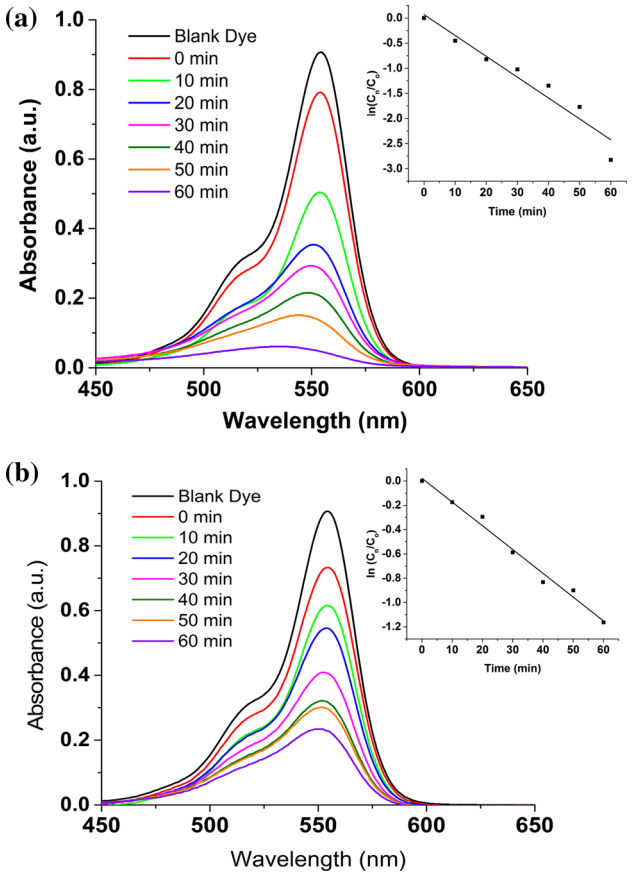

Figure 5 Photodegradation of Rhodamine B using **a** ZnO formed by co-precipitation route (ZNO2) and **b** ZnO formed as an assembly of particles to form rods (ZNO3). The inset shows the plot showing that the catalysis followed first-order kinetics.

these spherical particles was ~ 50–100 nm (Inset of figure S4a). In case of ZNO3, particles assembled to form rods (figure S4b) which degraded 75% of Rhodamine B in 60 min with a rate constant of 0.019 min^{-1} (Fig. 5b). Based on the above results, it is to be noted that among the three different kinds of nanostructures of ZnO that were studied, viz. spherical particles, particles assembled to form hollow structures and particles assembled to form rods, it was observed that the hollow nanostructures were more effective for photodegradation of Rhodamine B. Thus, it can be concluded that the nature of assembly is an important factor in governing the photocatalytic activity. The reason for achieving the photocatalytic degradation of the dye for ZNO1 in less time could be attributed to the hollow nature of the assembly of nanoparticles. It has been reported [30] that photons get trapped inside the hollow structure when light shines on the structure while a few photons get reflected back. Trapped photons lead to the generation of more number of e^{-}-h^{+} pairs, thereby increasing the photocatalytic efficiency. This could be the reason for the observed higher efficiency of the assembly of ZnO nanoparticles to form hollow structures toward photodegradation of Rhodamine B and methyl orange.

We list here few reports from the literature on photocatalytic studies for degradation of dye using hollow ZnO. Wu et al. [31] showed that 1 mg mL^{-1} of ZnO hollow shell degraded a solution of 50 μM of Rhodamine B in 135 min. Zhang et al. [19] showed that when ZnO hollow shells were formed using two-step approach, a solution containing 20 mg L^{-1} of methylene blue was degraded to 50% of the initial concentration in 90 min with 0.25 mg mL^{-1} of the catalyst. However, the degradation was complete in the same time when ZnO hollow shells were formed using a one-step approach. In another study, the time

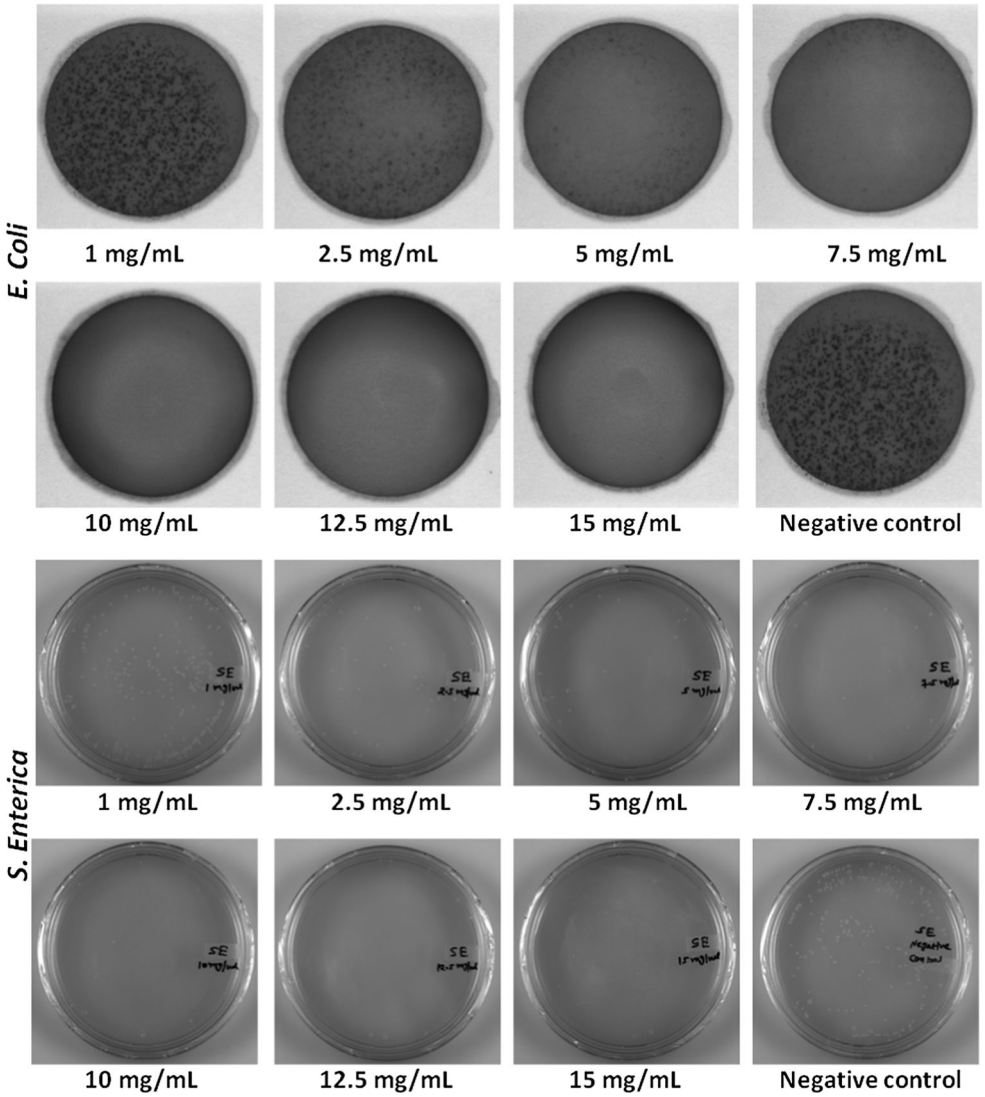

Figure 6 Optical images of inhibition in bacterial colonies in 3 M Petri film *E. Coli* count (EC) plates (*E. coli)* and LB agar plate medium *(S. Enterica*) after treatment with ZNO1.

taken for complete degradation of Rhodamine B dye (10 mg L^{-1}) was 150 min using 0.6 mg mL^{-1} of ZnO hollow shells [30]. Mahjoub et al. [32] studied the photodegradation of Congo red dye (20 ppm) using 0.2 mg mL^{-1} of the catalyst (hollow ZnO) and found the degradation was close to 99% for one of the catalysts. In a similar kind of study carried out by Gan et al. [33], it was observed that 65% of Congo red (100 mg L^{-1}) was degraded by hollow ZnO (0.5 g L^{-1}). Hollow cocoons of ZnO synthesized by Pal et al. [34] were effective in the degradation of Rhodamine B in 300 min. When an aqueous solution of Rhodamine B dye (10 μM) was photodegraded by Yu et al. [35] in the presence of hollow shells of ZnO (amount of catalyst: 0.2 mg mL^{-1}), complete degradation of Rhodamine B dye was achieved in 4 h. In our study, a 9 μM solution of Rhodamine B dye was degraded in 60 min and 12 μM solution of methyl orange in 50 min by the hollow ZnO with a catalyst concentration of 1 mg mL^{-1}. The above studies show that the assembly of nanoparticles to form hollow ZnO discussed in this paper was more effective in the photodegradation of Rhodamine B and methyl orange.

In vitro antibacterial activity

The antibacterial activity of ZnO nanostructures against *E. Coli* and *S. Enterica* was studied quantitatively by colony-forming unit using 3 M Petrifilm *E. Coli* count plates and LB agar plate method, respectively. In the present study, we tested different concentrations of ZnO nanostructure (ZNO1, ZNO2 and ZNO3), viz. 1, 2.5, 5, 7.5, 10, 12.5 and

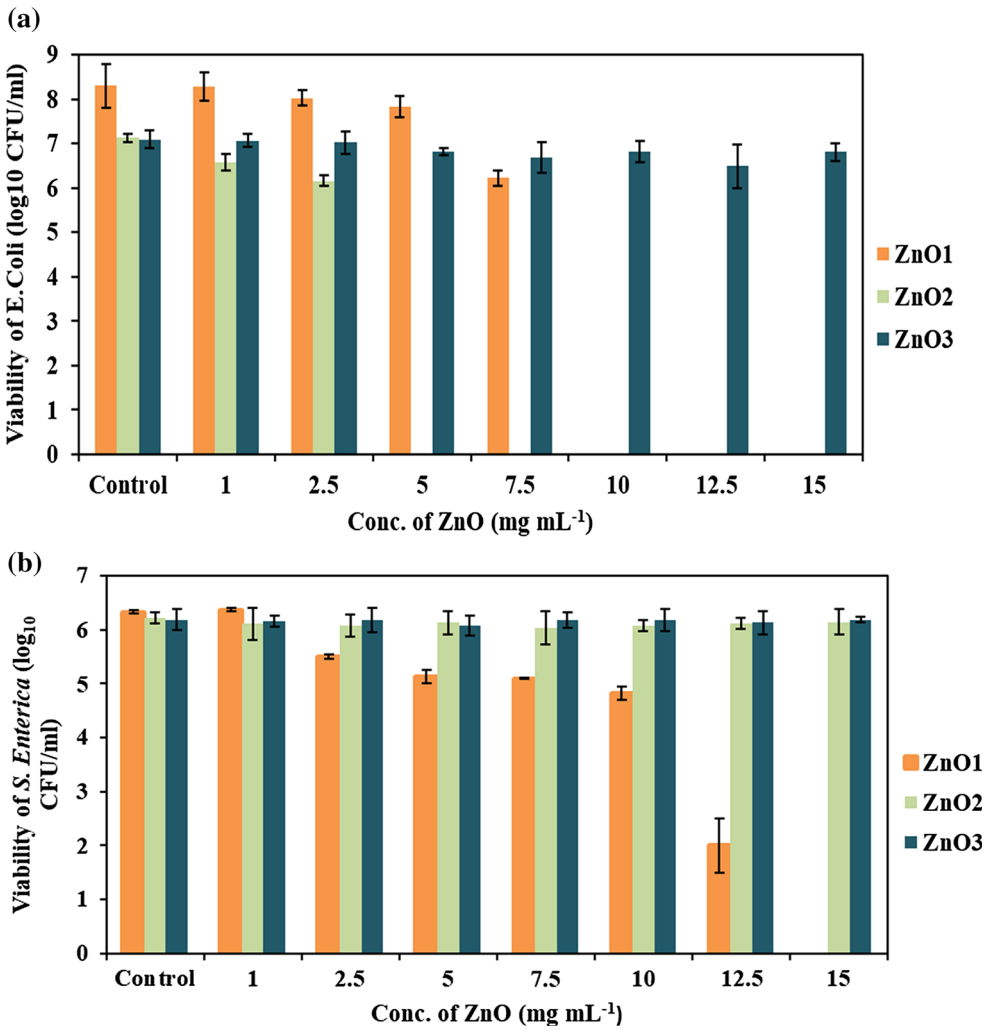

Figure 7 Graphical representation of reduction in the bacterial growth of **a** *E. coli* and **b** *S. Enterica* after treatment with different concentrations of ZnO nanostructures (ZNO1, ZNO2 and ZNO3).

15 mg mL^{-1}, and the reduction in the bacterial colony was evaluated after 6 h of incubation. As evident from Fig. 6 (optical images of bacteria in culture Petriplates) and Fig. 7a and 7b (CFU count), hollow assembly of ZNO1 demonstrated significant antibacterial activity against *E. Coli* and *S. Enterica* compared to ZNO2 and ZNO3. Notable suppression in the growth of *E. Coli* was observed at a concentration as low as ~ 1–7.5 mg mL^{-1}, whereas at higher concentration (10–15 mg mL^{-1}) complete inhibition was observed in ZNO1. To confirm the effect of the nature of assembly on the antibacterial activity, the studies were performed on ZNO2 and ZNO3. It was observed that for *E.Coli*, the bacterial inhibition of ZNO2 was found to be similar to that of ZNO1 (Fig. 7a and S5a). ZNO3, however, showed no bacterial growth inhibition for *E.Coli* (Fig. 7a and S5a). Suppression in the growth of *S. Enterica* was observed in the concentration range of 1–15 mg mL^{-1} in the presence of ZNO1, whereas bacterial growth inhibition was not observed in the presence of ZNO2 and ZNO3 (Fig. 7b and S5b). The reduction in bacterial growth after treatment with the ZnO structures for 6 h demonstrates that the antibacterial activity of the synthesized hollow ZnO nanostructure (ZNO1) was significantly greater than ZNO2, ZNO3, and untreated negative control. The possible mechanism behind the antibacterial activity of ZnO nanostructures involves disruption of the bacterial cell wall membrane. The higher rate of generation of surface reactive oxygen species from ZnO nanostructures may lead to the death of the bacteria.

There is a report on the study of antibacterial activity of ZnO by Patrinoiu et al. [36] which shows the minimum inhibitory concentration for solid spheres of ZnO as 62.5 μg mL^{-1} for *S. Aureus*. This MIC value decreased to 36.78 μg mL^{-1} when hollow shells of ZnO were used. In a similar kind of studies,

Suresh et al. [37] showed that ZnO mesoporous particles exhibited antibacterial activity with a concentration of 500 μg/50 μL and 1000 μg/100 μL. Suwanboon et al. [38] showed that the ZnO prepared by their group showed inhibitory actions for *S. Aureus* and did not have any effect on *E. Coli*. In our study, the growth of the bacteria was inhibited beyond 10 mg mL^{-1} for *E. Coli*, whereas the growth of *S. Enterica* was suppressed in the concentration range (1–15 mg mL^{-1}).

Conclusions

Hollow ZnO was prepared by the assembly of ZnO nanoparticles (50–60 nm) using PEG-400 as the structure directing agent. These assemblies were demonstrated to exhibit enhanced photocatalytic activity for the degradation of two dyes, viz. Rhodamine B and methyl orange. Nearly complete degradation of these two dyes was observed in an hour. The assemblies were found to be useful to suppress the growth of *E.Coli* and *S.Enterica* at low concentration of oxide. It was demonstrated that the growth of *E. Coli* was inhibited when 10 mg mL^{-1} of particles was used, whereas suppression in the growth of *S. Enterica* was observed in the presence of ZnO (1–15 mg mL^{-1}). Comparative studies were performed for showcasing the efficiency of these hollow nanostructured assemblies for photocatalytic and antibacterial activity. Our studies show that the hollow nature of the assembly was effective in removing dyes from water and inhibiting the growth of bacteria. The assembly thus was found to have a potential for water purification, coatings, food packaging industry, etc.

Acknowledgments

ZZ and AV thank INST for financial support. SV thanks DST, Govt. of India (SERB/F/4909/2013-14) and INST (25(1)/2015-INST) for financial support. The authors thank IISER Mohali for FESEM studies.

Electronic supplementary material: The online version of this article (https://doi.org/10.1007/s10853-018-2715-4) contains supplementary material, which is available to authorized users.

References

[1] Kim D, Huh Y-D (2011) Mater Lett 65:2100. https://doi.org/10.1016/j.matlet.2011.04.074

[2] Gupta J, Bhargava P, Bahadur D (2014) Physica B 448:16. https://doi.org/10.1016/j.physb.2014.03.081

[3] Hui A, Ma J, Liu J, Bao Y, Zhang J (2017) J Alloy Compd 696:639. https://doi.org/10.1016/j.jallcom.2016.10.319

[4] Wang Y, Li X, Wang N, Quan X, Chen Y (2008) Sep Purif Technol 62:727. https://doi.org/10.1016/j.seppur.2008.03.035

[5] Lu H, Wang S, Zhao L, Li J, Dong B, Xu Z (2011) J Mater Chem 21:4228. https://doi.org/10.1039/C0JM03390A

[6] Pung S-Y, Lee W-P, Aziz A (2012) Int J Inorg Chem 2012:9. https://doi.org/10.1155/2012/608183

[7] Xu L, Hu Y-L, Pelligra C et al (2009) Chem Mater 21:2875. https://doi.org/10.1021/cm900608d

[8] Sun H, Yu Y, Luo J, Ahmad M, Zhu J (2012) CrystEngComm 14:8626. https://doi.org/10.1039/C2CE26157J

[9] Rezapour M, Talebian N (2011) Mater Chem Phys 129:249. https://doi.org/10.1016/j.matchemphys.2011.04.012

[10] Vidovic S, Elder J, Medihala P et al (2015) Antimicrob Agents Chemother 59:3317. https://doi.org/10.1128/aac.00363-15

[11] Espitia PJP, NdFF Soares JSdR, de Coimbra NJ, Andrade RS Cruz, Medeiros EAA (2012) Food Bioprocess Technol 5:1447. https://doi.org/10.1007/s11947-012-0797-6

[12] Azam A, Ahmed AS, Oves M, Khan MS, Habib SS, Memic A (2012) Int J Nanomed 7:6003. https://doi.org/10.2147/IJN.S35347

[13] Li X, Xing Y, Jiang Y, Ding Y, Li W (2009) Int J Food Sci Technol 44:2161. https://doi.org/10.1111/j.1365-2621.2009.02055.x

[14] Padmavathy N, Vijayaraghavan R (2008) Sci Technol Adv Mater 9:035004. https://doi.org/10.1088/1468-6996/9/3/035004

[15] Raghupathi KR, Koodali RT, Manna AC (2011) Langmuir 27:4020. https://doi.org/10.1021/la104825u

[16] Talebian N, Amininezhad SM, Doudi M (2013) J Photochem Photobiol B 120:66. https://doi.org/10.1016/j.jphotobiol.2013.01.004

[17] Liu J, Rojas-Andrade MD, Chata G et al (2018) Nanoscale 10:158. https://doi.org/10.1039/C7NR07367D

[18] Zhang L-H, Sun Q, Liu D-H, Lu A-H (2013) J Mat Chem A 1:9477. https://doi.org/10.1039/C3TA10430C

[19] Zhang C, Yin L, Zhang L, Qi Y, Lun N (2012) Mater Lett 67:303. https://doi.org/10.1016/j.matlet.2011.09.073

[20] Patrinoiu G, Tudose M, Calderón-Moreno JM et al (2012) J Solid State Chem 186:17. https://doi.org/10.1016/j.jssc.2011.11.024

[21] Chen D, Ye J (2008) Adv Func Mater 18:1922. https://doi.org/10.1002/adfm.200701468
[22] Xia J, Yin S, Li H, Xu H, Yan Y, Zhang Q (2011) Langmuir 27:1200. https://doi.org/10.1021/la104054r
[23] Liu Y, Xu C, Zhu Z, Lu J, Manohari AG, Shi Z (2018) Mater Res Bull 98:64. https://doi.org/10.1016/j.materresbull.2017.09.057
[24] Cao S-W, Zhu Y-J (2008) J Phys Chem C 112:6253. https://doi.org/10.1021/jp8000465
[25] Chen JS, Chen C, Liu J, Xu R, Qiao SZ, Lou XW (2011) Chem Commun 47:2631. https://doi.org/10.1039/C0CC04471G
[26] Wang X, Liao M, Zhong Y et al (2012) Adv Mater 24:3421. https://doi.org/10.1002/adma.201201139
[27] Rao J, Yu A, Shao C, Zhou X (2012) ACS Appl Mater Interfaces 4:5346. https://doi.org/10.1021/am3012966
[28] Ahmad T, Vaidya S, Sarkar N, Ghosh S, Ganguli AK (2006) Nanotechnology 17:1236
[29] Karakoti AS, Das S, Thevuthasan S, Seal S (2011) Angew Chem Int Ed 50:1980. https://doi.org/10.1002/anie.201002969
[30] Zhu C, Lu B, Su Q, Xie E, Lan W (2012) Nanoscale 4:3060. https://doi.org/10.1039/C2NR12010K
[31] Deng Z, Chen M, Gu G, Wu L (2008) J Phys Chem B 112:16. https://doi.org/10.1021/jp077662w
[32] Mousavi SM, Mahjoub AR, Abazari R (2015) RSC Adv 5:107378. https://doi.org/10.1039/C5RA19507A
[33] Lan S, Liu L, Li R, Leng Z, Gan S (2014) Ind Eng Chem Res 53:3131. https://doi.org/10.1021/ie404053m
[34] Sinha AK, Basu M, Pradhan M, Sarkar S, Pal T (2010) Chem A Eur J 16:7865. https://doi.org/10.1002/chem.200903347
[35] Yu J, Yu X (2008) Environ Sci Technol 42:4902. https://doi.org/10.1021/es800036n
[36] Patrinoiu G, Calderón-Moreno JM, Chifiriuc CM, Saviuc C, Birjega R, Carp O (2016) J Colloid Interface Sci 462:64. https://doi.org/10.1016/j.jcis.2015.09.059
[37] Suresh D, Udayabhanu PC Nethravathi et al (2015) Spectrochim Acta Part A Mol Biomol Spectrosc 136:1467. https://doi.org/10.1016/j.saa.2014.10.038
[38] Suwanboon S, Klubnuan S, Jantha N, Amornpitoksuk P, Bangrak P (2014) Mater Lett 115:275. https://doi.org/10.1016/j.matlet.2013.10.066